Supplementary Materials

A survey of energies from pure metals to multi-principal element alloys

Ruitian Chen, Evelyn Li, Yu Zou*

Department of Materials Science and Engineering, University of Toronto, 184 College St, Toronto, ON M5S 3E4, Canada

***Correspondence to:** Prof. Yu Zou, Department of Materials Science and Engineering, University of Toronto, 184 College St, Toronto, ON M5S 3E4, Canada. E-mail: mse.zou@utoronto.ca.

The parameters used to calculate energies are listed below.

Supplementary Table 1. Parameters of fcc materials

	Ni	NiCo	NiFe	NiCoCr	NiCoFe	NiFeCr	NiCoFeCr	NiCoFeCrMn
lattice constant a (Å)	3.5238 [1]	3.534 [2]	3.595 [3]	3.559 [4]	3.569 [4]	3.59 [5]	3.592 [5]	3.594 [5]
melting point T_{M} (K)	1728 [1]	1735 [6]	1703 [6]	1690 [6]	1724 [6]	1664 [6]	1695 [6]	1553 [7]
Debye temperature θ_{D} (K)	477 [8]	437 [9]	425 [10]	490 [4]	415 [4]	448# [4]	476 [11]	299 [12]
Curie temperature T_{c} (K)	611 [13]	956 [13]	554 [13]	7 [13]	838 [13]	106 [13]	161 [13]	34 [13]
stacking fault energy γ_{SF} (J/m^2)	0.125 [14]	-0.012 [15]	0.105 [15]	-0.045 [15]	0.075 [15]	0.061 [16]	0.0278 [16]	0.0264 [16]
vacancy formation energy Q (eV)	1.47 [17]	1.75 [17]	1.70 [17]	1.82 [18]	1.60 [19]	1.65 [20]	1.83 [18]	1.66 [21]
surface energy γ (J/m^2)	1.938 [22]	2.161 [23]	1.998 [24]	2.231 [25]	2.059 [25]	2.343 [25]	2.23 [26]	2.26 [26]
shear modulus G (GPa)	76 [1]	84 [7]	62 [7]	90 [27]	68 [27]	79 [27]	86 [27]	81 [12]
Young's modulus E (GPa)	200 [1]	214 [27]	166 [7]	235 [27]	175 [27]	190 [27]	214 [27]	203 [12]

(Note: $^{\#}\theta_{\mathrm{D}}$ = 448 K is for NiFe-20Cr)

Supplementary Table 2. Parameters of hcp materials

	Ti	Zr	TiZr	TiZrHf	TiZrHfSc
lattice constant a (Å)	2.954 [28]	3.232 [29]	3.1141 [30]	3.318 [31]	3.147 [31]
lattice constant c (Å)	4.685 [28]	5.147 [29]	4.9221 [30]	4.958 [31]	5.05 [31]
shear modulus G (GPa)	41.4 [32]	33.8 [33]	33.5 [34]	49.76 [31]	52.97 [31]
Young's modulus E (GPa)	105 [35]	91 [33]	90.5 [30]	96.9 [31]	90.72 [31]

Supplementary Table 3. Parameters of bcc materials

	W	Mo	NbMo	NbMoTa	NbMoTaW	NbMoTaWV
lattice constant a (Å)	3.158 [36]	3.1468 [36]	3.224 [37]	3.26 [38]	3.195 [39]	3.167 [39]
surface energy γ (J/m^2)	2.83 [40]	2.05 [40]	2.518 [41]	2.31	2.661 [41]	2.46
shear modulus G (GPa)	161 [36]	126 [36]	82.57	51.87 [38]	102 [39]	94 [39]
Young's modulus E (GPa)	410 [42]	329 [42]	280.6 [37]	143.69 [38]	270 [39]	249 [39]

The various parameter values for the metals and alloy used to calculate these energies are sourced from a broad range of literatures. Differential scanning calorimetry (DSC) is used to quantify melting points for several Ni-based alloys, while shear and Young's modulus values are acquired using techniques such as resonant ultrasound spectroscopy and estimated from wave velocities. Lattice constants are determined using X-ray diffraction (XRD) and crystallographic databases, whereas Debye temperatures are derived from specific heat measurements and theoretical computations. Density functional theory (DFT) is extensively employed, especially when calculating the surface energies, vacancy formation energies, and other properties. Additionally, complex alloys are studied through methods like the special quasi-random structure (SQS) technique and virtual crystal approximation (VCA). Detailed methods are listed below:

1. Fcc materials

1.1. Lattice constant

- **Ni, NiCoCr, NiCoFe:** CRC Handbook and database [1,4].
- **NiCo**: Crystallographic data on electrodeposited phases and thin films [2].
- **NiFe**: Determined by XRD [3].
- **NiFeCr, NiCoFeCr, NiCoFeCrMn:** computed through supercells and replaced Ni by Co, Fe, Cr, and Mn simultaneously to build the crystal structure of the studied alloys [5].

1.2. Melting point

- **Ni:** CRC Handbook [1].
- **NiCo, NiFe, NiCoCr, NiCoFe, NiFeCr, NiCoFeCr, and NiCoFeCrMn:** Differential scanning calorimetry (DSC) measurements [6,7].

1.3. Debye temperature

- **Ni, NiCo:** Specific heat measurements [8,9].
- **NiFe:** Calculated from the shear and young's modulus measurements [10].
- **NiCoCr, NiCoFe, NiFeCr:** Calculated from atomic volume and the mean sound velocity [4].
- **NiCoFeCr, NiCoFeCrMn:** Database [11,12].

1.4. Curie temperature

- **Ni, NiCo, NiFe, NiCoCr, NiCoFe, NiFeCr, NiCoFeCr, and NiCoFeCrMn:** Calculation within the mean field approximation [13].

1.5. Stacking fault energy

- **Ni:** Anisotropic elasticity theory [14].
- **NiCo, NiFe, NiCoCr, NiCoFe, NiFeCr, NiCoFeCr, NiCoFeCrMn:** First-principles and DFT calculations [15,16].

1.6. Vacancy formation energy

- **Ni, NiCo, NiFe:** Computed through finite-size models while comparing to ab initio calculations to those obtained from available embedded atom method (EAM) potentials [17].
- **NiCoFe:** DFT calculations based on the Similar Atomic Environment (SAE) method [19].
- **NiFeCr:** Computed from atomistic calculations [20].
- **NiCoCr, NiCoFeCr:** DFT calculation on special quasi-random structures (SQSs) [18].
- **NiCoFeCrMn:** DFT supercell calculations [21].

1.7. Surface energy

- **Ni:** Computed through model which was conducted by a combination of Monte Carlo (MC), molecular dynamics (MD) and lattice statics (LS) types of simulations [22].
- **NiCo:** Taken from the weighted average of the measurement of surface tensions of molten Co–Ni alloys experimentally, also verified through theoretical calculations [23].
- **NiFe:** DFT calculations with dispersion correction [24].
- **NiCoCr, NiCoFe, NiFeCr:** DFT calculations verified through thermodynamic modeling and a bond-cutting model [25].
- **NiCoFeCr, NiCoFeCrMn:** DFT calculations performed using the Vienna ab initio Simulation Package (VASP) within the generalized gradient approximation (GGA) and with the Perdew-Burke-Ernzerhof (PBE) functional, also with the use of projector augmented wave (PAW) method [26].

1.8. Shear modulus

- **Ni:** CRC Handbook [1].
- **NiCo, NiFe:** Measured in ultrasonic techniques - resonant ultrasound spectroscopy [7].
- **NiCoCr, NiCoFe, NiFeCr, NiCoFeCr, NiCoFeCrMn:** Determined using torsional deformation of plates [12,27].

1.9. Young's modulus

- **Ni:** CRC Handbook [1].
- **NiFe:** Calculated from shear modulus and Poisson's ratio [7].
- **NiCo, NiCoCr, NiCoFe, NiFeCr, NiCoFeCr, NiCoFeCrMn:** The ASTM E1876-01 standard test method [12,27].

2. Hcp materials

2.1. Lattice constant

- **Ti:** Calculated by DFT based on the CASTEP [28].
- **Zr:** Special quasi-random structure (SQS) technique implemented in the Alloy Theoretic Automated Toolkit (ATAT) [29].
- **TiZr:** Determined by XRD [30].
- **TiZrHf, TiZrHfSc:** SQS - energy versus volume (E–V) curve fitting with the 3rd Birch–Murnaghan equation of state [31].

2.2. Shear modulus & Young's modulus

- **Ti:** Database [32,35].
- **Zr:** DFT on the basis of the frozen-core projected augmented wave (PAW) method of Blochl are performed within the Vienna ab initio simulation package (VASP), where the Perdew,

Burke, and Ernzerhof (PBE) form of the generalized gradient approximation (GGA) is employed [33].

- **TiZr: Shear modulus:** measuring the velocities of ultrasonic sound waves traveling in the samples. 40 **/Young's modulus:** Compressive mechanical properties were evaluated by testing machine (SANS CMT5504) [30].
- **TiZrHf, TiZrHfSc:** DFT, SQS for pristine structure [31].

3. Bcc materials

3.1. Lattice constant

- **W, Mo:** From experimentally determined atomic radius [36].
- **NbMo:** Determined by XRD [37].
- **NbMoTa:** DFT calculations [38].
- **NbMoTaW, NbMoTaWV:** Virtual crystal approximate (VCA) method [39].

3.2. Surface energy

- **W, Mo:** Used multiphase equilibration, computed from experimental values (experimental values are from geometric changes produced by vectorial interaction at intersecting interfaces) [40].
- **NbMo, NbMoTaW:** DFT calculations using the SQS supercells [41].
- **NbMoTa:** DFT calculations.

3.3. Shear modulus & Young's modulus

- **W, Mo:** Database [36,42].
- **NbMo: Shear modulus:** DFT. **/Young's modulus:** Oliver and Pharr method (indentation tests) [42].
- **NbMoTa:** DFT calculations [38].
- **NbMoTaW, NbMoTaWV:** Virtual crystal approximate (VCA) method [39].

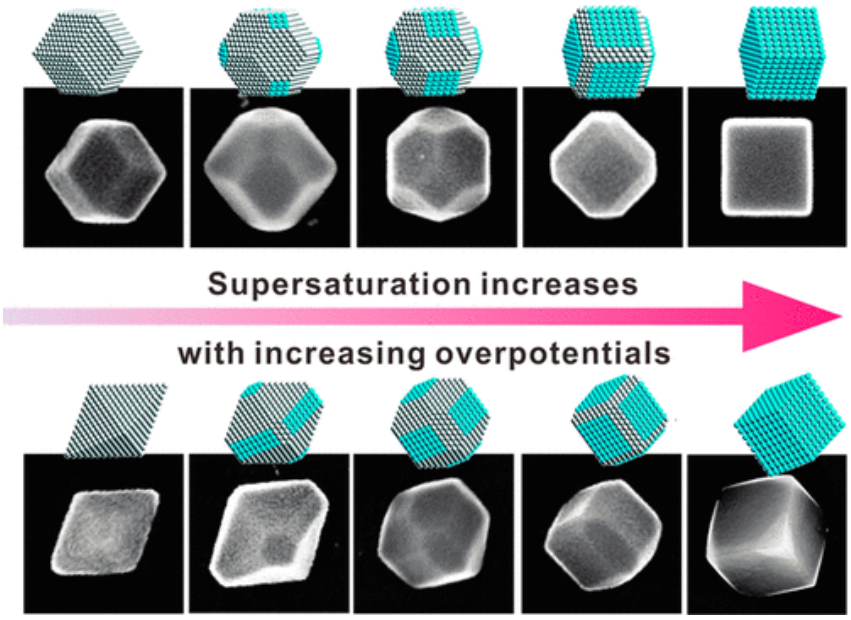

Supplementary Figure 1. Shape evolution of two series of Fe NCs from low-energy (110) facets to high-energy (100) facets with increasing the overpotential. Gray color, (110) facet; cyan color, (100) facet. Reprinted with permission from Ref. [43]. Copyright (2018) American Chemical Society.

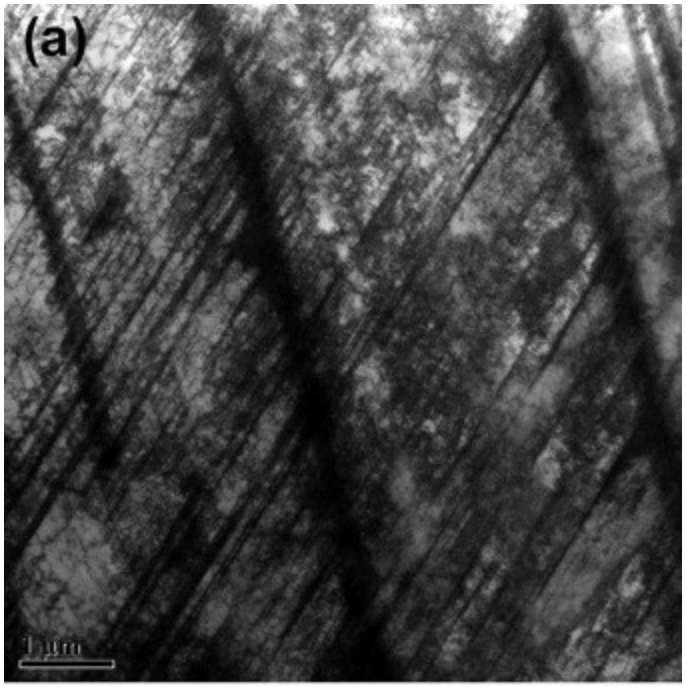

Supplementary Figure 2. Dark-field TEM image showing a high dislocation density of ~10^{16} m^{-2} in NiCoFeCrMn high-entropy alloy (Ref. [44]). Copyright (2020), with permission from Elsevier.

References

[1] Lide DR. CRC handbook of chemistry and physics. *CRC press* 2004.

[2] Nishizawa T, Ishida K. The Co−Ni (Cobalt-Nickel) system. *Bulletin of Alloy Phase Diagrams* 1983;4:390. [DOI: 10.1007/BF02868090]

[3] Guittoum A; Layadi A; Bourzami A et al. X-ray diffraction, microstructure, Mössbauer and magnetization studies of nanostructured Fe50Ni50 alloy prepared by mechanical alloying. *J Magn Magn Mater* 2008;320:1385. [DOI: 10.1016/j.jmmm.2007.11.021]

[4] Jin K; Gao YF; Bei H. Intrinsic properties and strengthening mechanism of monocrystalline Ni-containing ternary concentrated solid solutions. *Materials Science and Engineering: A* 2017;695:74. [DOI: 10.1016/j.msea.2017.04.003]

[5] Ali ML; Haque E; Rahaman MZ. Pressure- and temperature-dependent physical metallurgy in a face-centered cubic NiCoFeCrMn high entropy alloy and its subsystems. *J.Alloys Compounds* 2021;873:159843. [DOI: 10.1016/j.jallcom.2021.159843]

[6] Wu Z; Bei H; Otto F; Pharr GM; George EP. Recovery, recrystallization, grain growth and phase stability of a family of FCC-structured multi-component equiatomic solid solution alloys. *Intermetallics* 2014;46:131. [DOI: 10.1016/j.intermet.2013.10.024]

[7] Wu Z; Bei H; Pharr GM; George EP. Temperature dependence of the mechanical properties of equiatomic solid solution alloys with face-centered cubic crystal structures. *Acta Materialia* 2014;81:428. [DOI: 10.1016/j.actamat.2014.08.026]

[8] Stewart GR. Measurement of low-temperature specific heat. *Rev.Sci.Instrum.* 1983;54:1. [DOI: 10.1063/1.1137207]

[9] Tóth BG; Péter L; Révész Á; Pádár J; Bakonyi I. Temperature dependence of the electrical resistivity and the anisotropic magnetoresistance (AMR) of electrodeposited Ni-Co alloys. *The European Physical Journal B* 2010;75:167. [DOI: 10.1140/epjb/e2010-00132-4]

[10] Tanji Y. Debye Temperature and Lattice Deviation of Fe-Ni (fcc) Alloys. *J.Phys.Soc.Jpn.* 1971;30:133. [DOI: 10.1143/JPSJ.30.133]

[11] Anderson OL. A simplified method for calculating the debye temperature from elastic constants. *Journal of Physics and Chemistry of Solids* 1963;24:909. [DOI: 10.1016/0022-3697(63)90067-2]

[12] Laplanche G; Gadaud P; Horst O; Otto F; Eggeler G; George EP. Temperature dependencies of the elastic moduli and thermal expansion coefficient of an equiatomic, single-phase CoCrFeMnNi high-entropy alloy. *J.Alloys Compounds* 2015;623:348. [DOI: 10.1016/j.jallcom.2014.11.061]

[13] Ge H; Song H; Shen J; Tian F. Effect of alloying on the thermal-elastic properties of 3d high-entropy alloys. *Mater.Chem.Phys.* 2018;210:320. [DOI: 10.1016/j.matchemphys.2017.10.046]

[14] Carter CB, Holmes SM. The stacking-fault energy of nickel. *The Philosophical Magazine: A Journal of Theoretical Experimental and Applied Physics* 1977;35:1161. [DOI: 10.1080/14786437708232942]

[15] Zhao S; Stocks GM; Zhang Y. Stacking fault energies of face-centered cubic concentrated solid solution alloys. *Acta Materialia* 2017;134:334. [DOI: 10.1016/j.actamat.2017.05.001]
[16] Zaddach AJ; Niu C; Koch CC; Irving DL. Mechanical Properties and Stacking Fault Energies of NiFeCrCoMn High-Entropy Alloy. *JOM* 2013;65:1780. [DOI: 10.1007/s11837-013-0771-4]
[17] Zhao S; Stocks GM; Zhang Y. Defect energetics of concentrated solid-solution alloys from ab initio calculations: Ni0.5Co0.5, Ni0.5Fe0.5, Ni0.8Fe0.2 and Ni0.8Cr0.2. *Phys.Chem.Chem.Phys.* 2016;18:24043. [DOI: 10.1039/C6CP05161H]
[18] Manzoor A; Zhang Y; Aidhy DS. Factors affecting the vacancy formation energy in Fe70Ni10Cr20 random concentrated alloy. *Computational Materials Science* 2021;198:110669. [DOI: 10.1016/j.commatsci.2021.110669]
[19] Guan H; Huang S; Tian F; Lu C; Xu Q; Zhao J. Universal enhancement of vacancy diffusion by Mn inducing anomalous Friedel oscillation in concentrated solid-solution alloys. *arXiv preprint arXiv:2303.15172* 2023[DOI: 10.48550/arXiv.2303.15172]
[20] Manzoor A; Arora G; Jerome B; Linton N; Norman B; Aidhy DS. Machine Learning Based Methodology to Predict Point Defect Energies in Multi-Principal Element Alloys. *Frontiers in Materials* 2021;8:[DOI: 10.3389/fmats.2021.673574]
[21] Razumovskiy VI; Scheiber D; Peil O; Stark A; Mayer M; Ressel G. Thermodynamics of Vacancy Formation in the CoCrFeMnNi High Entropy Alloy from DFT Calculations. *Aspects Min Miner Sci.* 2022;8:962. [DOI: 10.31031/AMMS.2022.08.000699]
[22] Wynblatt P, Chatain D. Modeling grain boundary and surface segregation in multicomponent high-entropy alloys. *Phys.Rev.Mater.* 2019;3:054004. [DOI: 10.1103/PhysRevMaterials.3.054004]
[23] Takrori FM, Ayyad A. Surface energy of metal alloy nanoparticles. *Appl.Surf.Sci.* 2017;401:65. [DOI: 10.1016/j.apsusc.2016.12.208]
[24] He Y; Jia J; Wu H. First-Principles Investigation of the Molecular Adsorption and Dissociation of Hydrazine on Ni–Fe Alloy Surfaces. *J.Phys.Chem.C* 2015;119:8763. [DOI: 10.1021/acs.jpcc.5b01605]
[25] Li W; Peng X; Ngan AHW; El-Awady J. Surface energies and relaxation of NiCoCr and NiFeX (X = Cu, Co or Cr) equiatomic multiprincipal element alloys from first principles calculations. *Modell Simul Mater Sci Eng* 2021;30:025001. [DOI: 10.1088/1361-651X/ac3e07]
[26] Zhou X, Curtin WA. First principles study of the effect of hydrogen in austenitic stainless steels and high entropy alloys. *Acta Materialia* 2020;200:932. [DOI: 10.1016/j.actamat.2020.09.070]
[27] Laplanche G; Gadaud P; Bärsch C et al. Elastic moduli and thermal expansion coefficients of medium-entropy subsystems of the CrMnFeCoNi high-entropy alloy. *J.Alloys Compounds* 2018;746:244. [DOI: 10.1016/j.jallcom.2018.02.251]
[28] Hao PD; Chen P; Deng L et al. Anisotropic elastic and thermodynamic properties of the HCP-Titanium and the FCC-Titanium structure under different pressures. *Journal of Materials Research and Technology* 2020;9:3488. [DOI: 10.1016/j.jmrt.2020.01.086]

[29] Liu Y, Zheng G. First-Principles Calculation and Kink-Dislocation Dynamics Simulation on Dislocation Plasticity in TiZr-Based Concentrated Solid-Solution Alloys. *Metals* 2023;13:[DOI: 10.3390/met13020351]
[30] Bao X; Li X; Ding J; Liu X; Meng M; Zhang T. Exploring the limits of mechanical properties of Ti-Zr binary alloys. *Mater Lett* 2022;318:132091. [DOI: 10.1016/j.matlet.2022.132091]
[31] Meng H; Duan J; Chen X; Jiang S; Shao L; Tang B. Influence of Local Lattice Distortion on Elastic Properties of Hexagonal Close-Packed TiZrHf and TiZrHfSc Refractory Alloys. *Phys.Status Solidi B* 2021;258:2100025. [DOI: 10.1002/pssb.202100025]
[32] Archer RR, Lardner TJ. An Introduction to the Mechanics of Solids. *McGraw-Hill* 1978.
[33] Wang B; Zhang P; Liu H; Li W; Zhang P. First-principles calculations of phase transition, elastic modulus, and superconductivity under pressure for zirconium. *Journal of Applied Physics* 2011;109:063514. [DOI: 10.1063/1.3556753]
[34] Shiraishi T; Yubuta K; Shishido T; Shinozaki N. Elastic Properties of As-Solidified Ti-Zr Binary Alloys for Biomedical Applications. *MATERIALS TRANSACTIONS* 2016;57:1986. [DOI: 10.2320/matertrans.MI201501]
[35] Mohammed MT; Khan ZA; Siddiquee AN. Titanium and its alloys, the imperative materials for biomedical applications. *International Conference on Recent Trends in Engineering & Technology* 2012
[36] Li Q; Zhang H; Li D; Chen Z; Qi Z. The effect of configurational entropy on mechanical properties of single BCC structural refractory high-entropy alloys systems. *International Journal of Refractory Metals and Hard Materials* 2020;93:105370. [DOI: 10.1016/j.ijrmhm.2020.105370]
[37] Panina E; Yurchenko N; Tojibaev A; Mishunin M; Zherebtsov S; Stepanov N. Mechanical properties of (HfCo)100−x(NbMo)x refractory high-entropy alloys with a dual-phase bcc-B2 structure. *J.Alloys Compounds* 2022;927:167013. [DOI: 10.1016/j.jallcom.2022.167013]
[38] Mubassira S; Jian W; Xu S. Effects of Chemical Short-Range Order and Temperature on Basic Structure Parameters and Stacking Fault Energies in Multi-Principal Element Alloys. *Modelling* 2024;5:366. [DOI: 10.3390/modelling5010019]
[39] Hu YL; Bai LH; Tong YG et al. First-principle calculation investigation of NbMoTaW based refractory high entropy alloys. *J.Alloys Compounds* 2020;827:153963. [DOI: 10.1016/j.jallcom.2020.153963]
[40] Hodkin EN; Nicholas MG; Poole DM. The surface energies of solid molybdenum, niobium, tantalum and tungsten. *Journal of the Less Common Metals* 1970;20:93. [DOI: 10.1016/0022-5088(70)90093-7]
[41] Hu Y; Sundar A; Ogata S; Qi L. Screening of generalized stacking fault energies, surface energies and intrinsic ductile potency of refractory multicomponent alloys. *Acta Materialia* 2021;210:116800. [DOI: 10.1016/j.actamat.2021.116800]
[42] Hua G, Li D. Generic relation between the electron work function and Young's modulus of metals. *Appl.Phys.Lett.* 2011;99:041907. [DOI: 10.1063/1.3614475]

[43] Zhang J; Li H; Kuang Q; Xie Z. Toward Rationally Designing Surface Structures of Micro- and Nanocrystallites: Role of Supersaturation. *Acc.Chem.Res.* 2018;51:2880. [DOI: 10.1021/acs.accounts.8b00344]
[44] Naeem M; He H; Harjo S et al. Extremely high dislocation density and deformation pathway of CrMnFeCoNi high entropy alloy at ultralow temperature. *Scr.Mater.* 2020;188:21. [DOI: 10.1016/j.scriptamat.2020.07.004]